Journal of Power Sources 262 (2014) 10–14

Contents lists available at ScienceDirect

Journal of Power Sources

journal homepage: www.elsevier.com/locate/jpowsour

Short communication

Synthesis of nanosized mesoporous silicon by magnesium-thermal method used as anode material for lithium ion battery

Hai Zhong, Hui Zhan*, Yun-Hong Zhou

College of Chemistry and Molecular Sciences, Wuhan University, Wuhan, 430072, China

HIGHLIGHTS

- Mesoporous nano-silicon was obtained by magnesium thermal method and HF etching.
- The mesoporous nano-Si released the capacity above 1400 mAh g^{-1} after 100 cycles.
- Good performance was obtained without architecture optimization.

ARTICLE INFO

Article history:
Received 18 January 2014
Received in revised form
7 March 2014
Accepted 22 March 2014
Available online 30 March 2014

Keywords:
Magnesium thermal reduction
Nanosized mesoporous silicon
Silica
Anode material
Lithium ion battery

ABSTRACT

Magnesium thermal reduction of the silica aggregation following with HF etching is used to obtain mesoporous nano-Silicon. The product shows an 1844 mAh g^{-1} discharge capacity in the first cycle with 400 mA g^{-1} current density and it still delivers a 1444 mAh g^{-1} capacity after 100 cycles. Additionally, it presents a good rate capability. The mesoporous morphology and the ultra-fine particle are the reasons of the good electrochemical property.

1. Introduction

Silicon is the most promising candidate for the anode material to replace the conventional carbon-based anode in lithium ion battery (LIB), due to the largest theoretical capacity [1] ($Li_{22}Si_5$, ~4200 mAh g^{-1}), and the electrochemical alloy/de-alloy reaction voltage of below 0.5 V (vs. Li/Li^+) [2]. However, its large-scale application has been greatly hindered by the huge volume change [3] (up to 400%) during the repeated charge/discharge process, which has been believed to be the origin of the particle pulverization. Additionally, the volume expansion/shrinkage brings about a deterioration in electrical contact [4] and the appearance of "dead" silicon, which finally results in the electrode disintegration and the rapid capacity fading.

A number of strategies have been implemented to suppress the volume change and enhance or maintain the electric contact between silicon and the conductive agent. Examples include silicon nanowires [5], silicon nanotubes [6], porous silicon [7], and Si dispersed in an active/inactive matrix [8,9]. However, the report about the mesoporous nano-Si is rare. Recently, chemical reduction method has attracted much attention, especially the magnesium thermal reduction process to convert SiO_2 into Si [10]. Despite the good result obtained on Si anode material, it remains a very challenging topic to prepare the nanosized mesoporous silicon anode with good electrochemical performance.

In this work, mesoporous nano-silicon was obtained by a simple preparation including the magnesium thermal reduction of SiO_2 followed by HF etching. The final product was characterized in terms of XRD, SEM, TEM measurement, and evaluated by the cycling test. The etching treatment was proved to be an effective way to further improve the electrochemical performance of nano-Si. The HF-etched mesoporous nano-silicon maintained a capacity

* Corresponding author. Tel.: +86 27 68756931; fax: +86 27 68754067.
E-mail address: zhanhui3620@126.com (H. Zhan).

http://dx.doi.org/10.1016/j.jpowsour.2014.03.108
0378-7753/

above 1400 mAh g^{-1} after 100 cycles and shows a capacity of 1100 mAh g^{-1} at 1 A g^{-1}.

2. Experimental

2.1. Synthesis

The nano-sized silica (SiO_2) sphere was synthesized by a modified Stöber process [11]. 5 mL tetraethyl orthosilicate (TEOS) was injected into the mixture of 20 mL deionized H_2O, 4 mL $NH_3 \cdot H_2O$ and 20 mL 2-propanol at room temperature under the magnetic stirring. After reacting for 2 h, the colloidal SiO_2 spheres were collected by centrifugation and washed by deionized water, then dried at 120 °C. Stoichiometric (1:2.2, molar ratio) amount of SiO_2 and Mg powder was mixed and ball-milled in *n*-hexane medium (Pulverisette 7 Premium line, FRITSCH) with Argon protection. After removing the residue solvent, the SiO_2/Mg composite was transferred into a tube furnace and further heated at 500 °C for 30 min under Ar/H_2 flow (volume ration = 9:1). The obtained brown-yellow powder was stored in 1 M HCl solution for 12 h to dissolve the magnesium compounds, then filtered by distilled water and dried under vacuum at 60 °C. The sample was named as "as-prepared". Another sample, with the name of "HF etch" was gained by treating the "as-prepared" sample with 8% HF (H_2O:ethanol, 5:1, v/v) solution for 24 h, during the period, a 30 min ultrasonic agitation was conducted for 3 times.

2.2. Electrochemical measurements

The silicon electrodes consisted of the active material (50 wt.%), acetylene black (30 wt.%) and polyacrylic acid binder (PAA, 20 wt.%). The mixture slurry was well-stirred and then coated onto a copper foil. The typical mass loading was about 1.5 mg cm^{-2}. The 2016 coin cell was fabricated by separating the Li anode and the Si cathode with a Celgard 2300 separator. The electrolyte was 1 M $LiPF_6$ dissolving in ethylene carbonate (EC)/dimethyl carbonate (DMC) (1:1, v/v), and it contained 10% fluoro-ethylene carbonate (FEC) additive. The cell was assembled in an Ar-filled glove box (MECABOX80-1"s", Switzerland).

The charging/discharging tests were conducted on Land battery cycler (Land Co. Ltd., China). Unless specified, the cells were cycled between 0.01 and 1.5 V at a 400 mA g^{-1} current rate. AC impedance measurements were performed on an Autolab electrochemical analyzer (Autolab PGSTAT30, Eco Chemie) in the frequency range of 10 kHz–100 mHz at an amplitude of 5 mV. The spectra were all collected at the OCV.

2.3. Characterization

X-ray diffraction (XRD) analysis was conducted with an XRD-6000 diffractometer (Shimadzu, Japan), using Cu $K\alpha_1$ radiation and a scan rate of 3° min^{-1}. The morphology was observed on a Quanta 200 scanning electron microscope (SEM, FEI company, Holland). High-resolution Transmission Electron Microscope (TEM) images were collected on JEM-2100F HR-TEM/EDS (FEG High Resolution Transmission Electron Microscope). N_2 adsorption–desorption curve was test by Micromeritics ASAP2020 Accelerated Surface Area and Porosimetry System.

3. Results and discussion

The SEM images of the silica synthesized from TEOS are shown in Fig. 1. Obviously, the primary particle, with the size of 250 nm, is composed of the aggregation of many smaller particles, and this architecture also creates many pores at the surface of the primary particle. The inset XRD pattern of SiO_2 shows a typical amorphous structure with a greatly widened diffraction peak at around 22°, agreeing well with the previous observation on nano-SiO_2 [12].

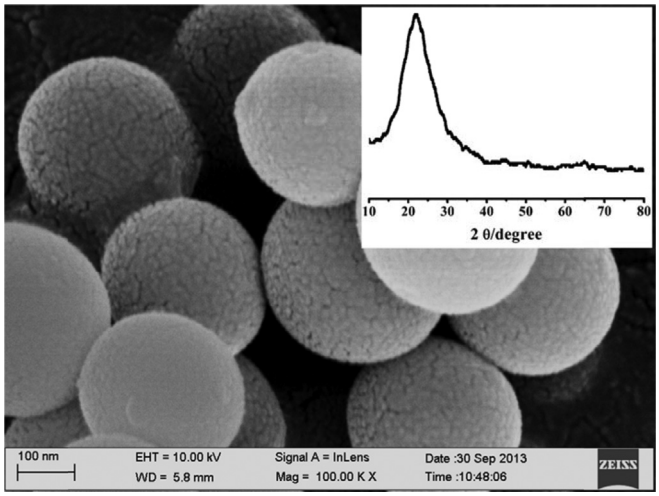

Fig. 1. SEM image and the XRD pattern (inset) of silica synthesized by tetraethyl orthosilicate (TEOS).

Fig. 2 compares the XRD pattern of the "as prepare" and "HF etch" sample. Very similar XRD patterns can be observed on the "as prepared" and "HF etch" sample, and most of the peaks can be indexed to Si according to JCPDS 27-1402, suggesting that SiO_2 has been mostly converted into Si. However, carefully comparing the diffraction peaks locating at around 22° and 28.5° of the two samples, we can notice that the peak intensity ratio of $I_{22°}/I_{28.5°}$ is higher for the "as-prepared" silicon than for the "HF etch" silicon. The result reveals that the "as prepared" sample contains more SiO_2 residue than the "HF etch" sample. The difference should be explained by the extra HF-etching procedure involved in the preparation of the "HF etch" sample.

The micrographs of the "as-prepared" and the "HF etch" silicon powder are compared in Fig. 3. In the SEM image of the "as-prepared" sample (Fig. 3a), we can see serious particle agglomeration. But after HF etching, the big agglomeration is well divided into small particles. In the SEM image of the "HF etch" sample (Fig. 3b), the granule with the 10–50 nm size and clear particle boundary can be observed. The difference is due to the

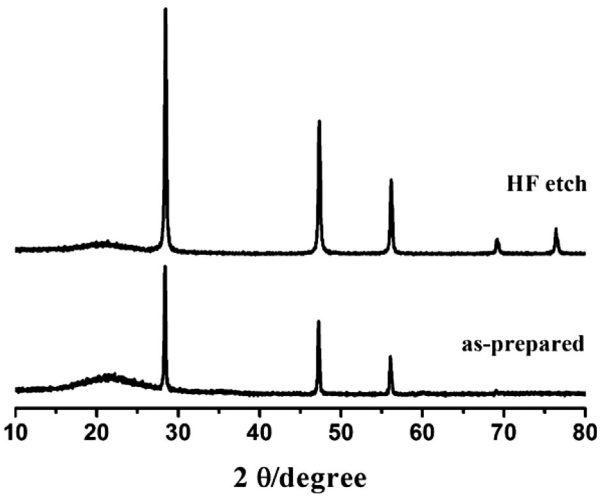

Fig. 2. XRD patterns of the "as prepared" silicon and the "HF etch" silicon sample.

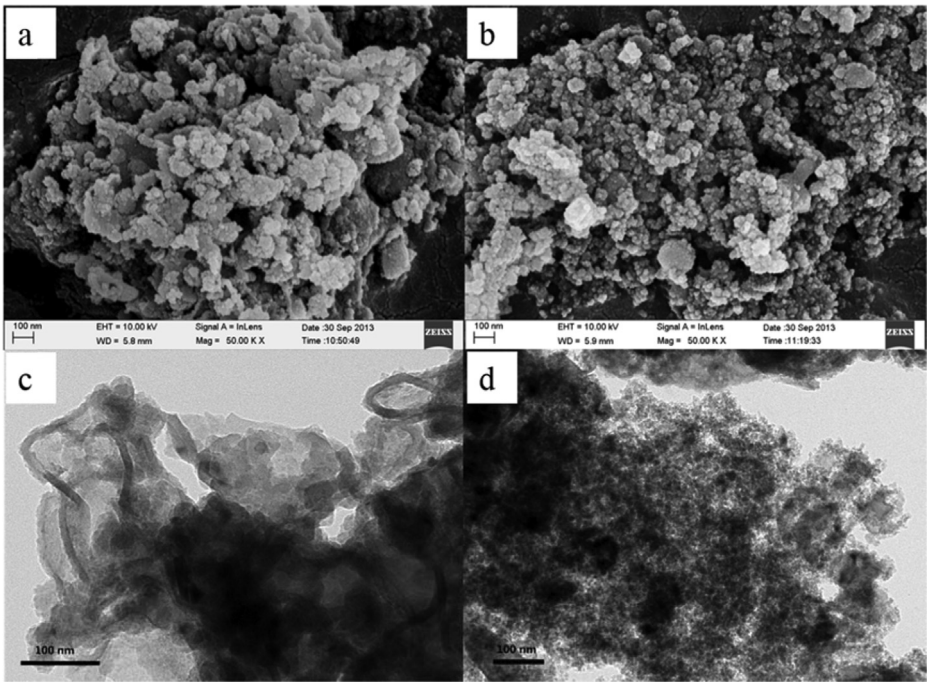

Fig. 3. SEM images of a) the "as prepared" silicon and b) the "HF etch" silicon; TEM images of the "as prepared" silicon c) and the "HF etch" silicon d).

dissolving effect of HF. As being proved in the XRD measurement, in the "as-prepared" sample, the amount of SiO_2 is still appreciable, and it may exist as a "bridge" between Si particles. The HF etching can effectively remove the SiO_2 "bridge" and make the nano-Si particle more discernable. Fig. 3c and d shows the TEM images of the "as-prepared" and "HF etch" sample respectively. The "as-prepared" sample had very different morphology from the "HF etch" sample. Sheet-like particles packed and wrapped together, and except near the edge of the particle, the mesoporous characteristic is not as obvious as in the "HF etch" sample. The mesoporous structure of the "HF etch" sample is also evidenced by the BET measurement. The specific surface area of the "HF etch" sample was 188.7 $m^2\ g^{-1}$ from nitrogen adsorption–desorption measurements. Nitrogen adsorption–desorption curves showed hysteresis at high relative pressure which was indicative of the mesoporous structure (Fig. 4). The pore size distribution calculated from the adsorption branch of the nitrogen isotherm by the BJH (Barrett–Joyner–Halenda) method indicated that the pore size was in the range of 2–40 nm, mostly smaller than 10 nm (see the inset of Fig. 4), and it is exhibited a bimodal pore size distribution. According to the SEM, TEM and BET experiment, it can be concluded that, after magnesium thermal reduction and further HF-etching, original silica aggregation was converted into nanocrystalline mesoporous silicon.

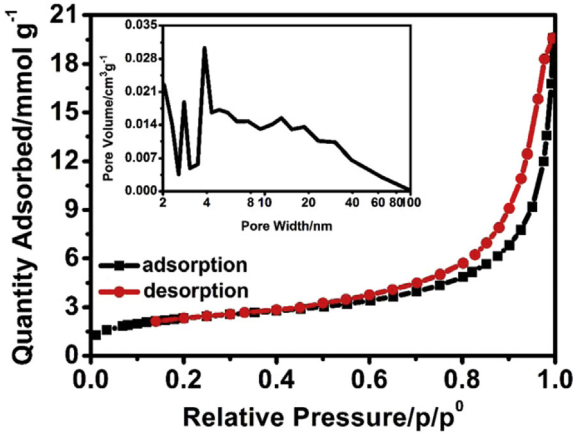

Fig. 4. N_2 adsorption and desorption isotherms of mesoporous "HF etch" silicon. Inset is the pore size distribution curve.

We tested the electrochemical properties of the two Si samples. In Fig. 5a, the "as-prepared" silicon sample delivers a 2585 mAh g^{-1} capacity in the 1st cycle at 400 mA g^{-1}, then the discharge capacity decreases rapidly until a 78% capacity drop after 100 cycles. Comparing with the "as-prepared" sample, the "HF etch" silicon sample gives a lower discharge capacity in the first cycle, but the capacity fades much more slowly and about 77% capacity can be reserved at 100th cycle. The capacity retention improvement in the "HF etch" silicon sample can be mainly explained by its particle morphology. As being mentioned above, serious particle agglomeration exists in the "as-prepared" silicon sample, and it will lead to an insufficient electrical contact between Si particles because of the volume change of Si during the charging/discharging. In order to get more clues of the better cycling stability of the "as-prepared" electrode than the "HF etch" electrode, their AC impedance is compared in Fig. 5b. In Fig. 5b, after 20 cycles, the "HF etch" electrode presents a smaller half-circle than the "HF etch" electrode in the high-frequency range, suggesting a smaller charge transfer resistance (R_{ct}). We think that the serious loss of electric contact in the "as prepared" electrode brings about a deteriorated reaction dynamics, which further cause a severe capacity fading. The loss of electric contact can be caused by two factors. First, due to the big volume change of Si, the big particle agglomeration in the "as prepared" sample makes it more difficult to maintain the original conductive network, such as the collection between Si particle and the contact between the Si electrode and the current collector [3]. Secondly, the larger SiO_2 amount in the "as prepared" sample than in the "HF etch" sample is another unignorable factor. Although the inactive SiO_2 can buffer the volume change in Si electrode during the alloying/de-alloying process to some extent, its existence can

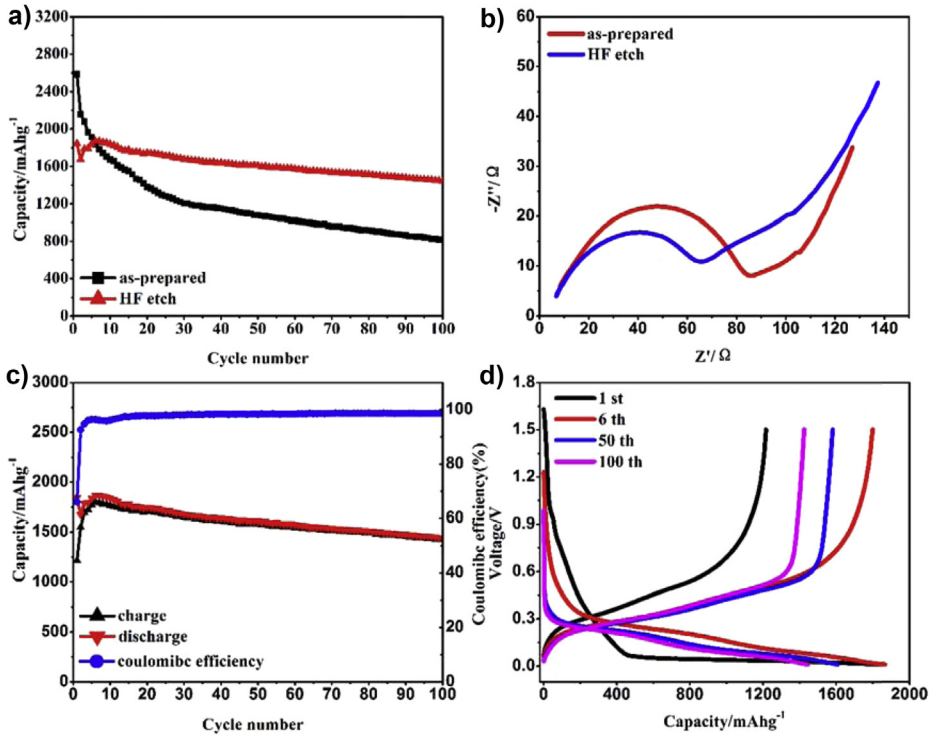

Fig. 5. a) Cycling stability of the "as-prepared" silicon and "HF etch" silicon at a current density of 400 mA g^{-1}; b) AC impedance of the "as-prepared" silicon and "HF etch" silicon electrode after 20 cycles; c) plot of charge and discharge capacity and Coulombic efficiency vs. cycles of the "HF etch" silicon; d) charge/discharge profiles of the "HF etch" silicon electrode at different cycle at a current density of 400 mA g^{-1}.

worsen the electron transfer when severe volume change occurs and the original conductive network is damaged. This is also the reason why in previous report, when the non-conductive component was used to composite with Si, a super fine particle and super uniform or complicated architecture was required [13]. In our "as prepared" sample, SiO_x is roughly distributed within Si particles to form some big agglomeration, and its beneficial buffering effect cannot be utilized; on the contrary, its insulating nature may play more negative effect on the Si electrode.

The plot of charge/discharge capacity and coulombic efficiency vs. cycles of the "HF etch" electrode is shown in Fig. 5c. In the first cycle, the discharge and charge capacity is 1844 mAh g^{-1} and 1216 mAh g^{-1} respectively, corresponding to the columbic efficiency of 66%. Both the discharge and charge capacity increases a little in the first few cycles. Similar observations were obtained previously on the nano-Si sample [14,15]. Actually, the formation process to completely activate the electrode material was widely observed in the mesoporous or microporous material [16,17] and was explained by the gradual electrolyte impregnation into the porous electrode. After the initial formation cycles, a maximum capacity of 1867 mAh g^{-1} is reached at the 6th cycle. Very slow capacity decay happens in the subsequent cycles, and the efficiency is kept constant at around 99%. The voltage profiles of the "HF etch" silicon electrode at different cycles are shown in Fig. 5d. We can see that except a significant polarization in the first cycle, the voltage hysteresis between the charge and the discharge plateau keeps small in the subsequent cycles, indicating a good maintaining of the reaction kinetics.

The SEM images of the fresh and cycled "HF etch" silicon electrode (100 cycles) are shown in Fig. 6a and b, respectively. In the fresh electrode, the mesoporous morphology can be well observed, while for the cycled "HF etch" electrode, the morphology information is mostly covered by the SEI layer. The growing SEI layer also "links" the particles together and makes them look bigger, but even that, we still can find many small pores on the surface of aggregates. Thus, we prefer to think that the mesoporous structure can be mostly retained after cycling.

To better understand the redox process of the "HF etch" electrode, a differential analysis was conducted on the 6th charge/discharge curve and the result is displayed in Fig. 7a. The alloying/de-alloying of lithium with Si leads to two pair of redox peaks at 0.29/0.08 V and 0.48/0.24 V vs. Li/Li^+, the observation agrees well with the previous report and should be attributed to the phase transition between different amorphous Li_xSi [18]. The small voltage segregation between the charge and discharge branch indicates good reaction reversibility. The "HF etch" electrode also exhibits an excellent rate capability, the voltage profiles at different current are shown in Fig. 7b. The capacity at the current of 0.1 A g^{-1} is 2046 mAh g^{-1}, and when the current is increased 10 times to 1 A g^{-1}, the electrode still presents a decent capacity of 1150 mAh g^{-1}. Even at 8 A g^{-1}, the electrode delivers an appreciable capacity of 322 mAh g^{-1}. It has to be noted that this performance is obtained without any component or architecture optimization in the sample, such as the introduction of conductive network into Si particles. We can expect a further enhanced performance after the adoption of other state-in-art strategy, and relative work is still in progress.

4. Conclusion

We synthesized mesoporous nano-silicon through thermally reducing the silica aggregation by Mg and a following HF etching. The final product delivers a capacity of 1867 mAh g^{-1} at the current rate of 400 mA g^{-1}, and it also exhibits an excellent cycling stability with a reversible capacity of 1444 mAh g^{-1} after 100 cycles and a decent rate performance. It has been proved that the mesoporous

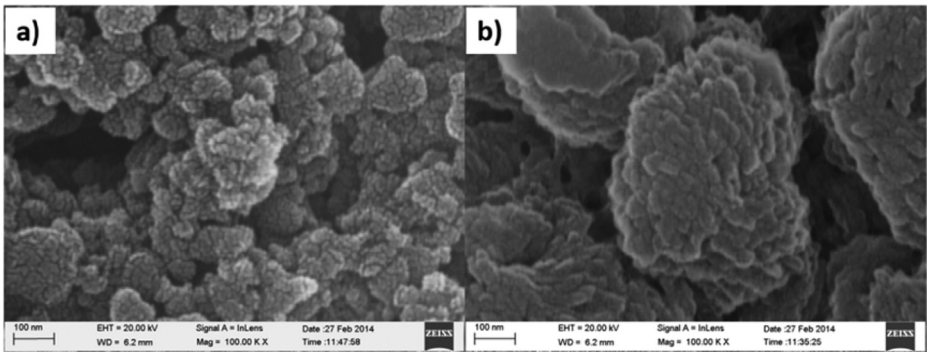

Fig. 6. The SEM images of a) fresh and b) cycled (100 cycles) "HF etch" silicon electrode.

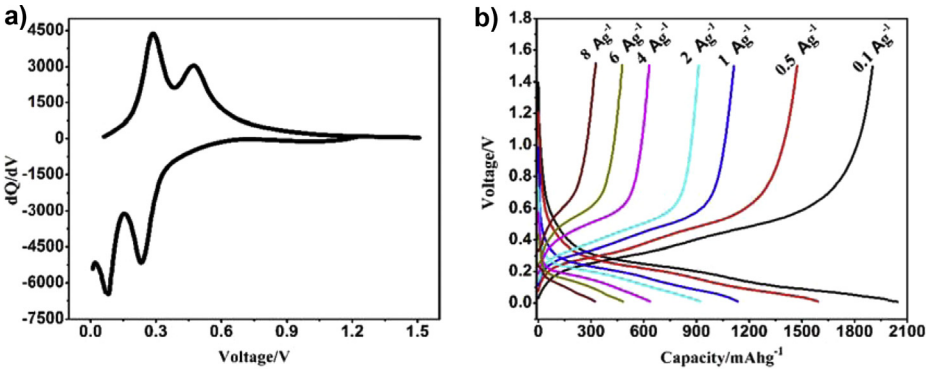

Fig. 7. a) d*Q*/d*V* curve of the "HF etch" silicon electrode at the 6th cycle; b) voltage profiles of the "HF etch" silicon electrode at the current density of 0.1, 0.5, 1, 2, 4, 6 and 8 A g^{-1}.

structure and the ultra-fine particle morphology are the main reasons for the good electrochemical properties.

Acknowledgments

Authors would express their sincere thanks to the Nature Science Foundation of China (No. 21073138, 21273168, 21233004) for the financial support.

References

[1] E. Radvanyi, E.D. Vito, W. Porcher, J. Danet, P. Desbois, J.F. Colin, S.J.S. Larbi, J. Mater. Chem. A 1 (2013) 4956–4965.
[2] H. Jung, M. Park, Y.G. Yoon, G.B. Kim, S.K. Joo, J. Power Sources 115 (2003) 346–351.
[3] J.H. Ryu, J.W. Kim, Y.E. Sung, S.M. Oh, Electrochem. Solid-state Lett. 7 (2004) A306–A309.
[4] X. Yang, Z. Wen, X. Xu, Z. Gu, S. Huang, Electrochem. Solid-state Lett. 10 (2007) A52–A55.
[5] C.K. Chan, H.L. Peng, G. Liu, K. Mcilwrath, X.F. Zhang, R.A. Huggins, Y. Cui, Nat. Nanotechnol. 3 (2008) 31–35.
[6] M.H. Park, M.G. Kim, J. Joo, K. Kim, J. Kim, S. Ahn, Y. Cui, J. Cho, Nano Lett. 9 (2009) 3844–3847.
[7] H.C. Shin, J.A. Corno, J.L. Gole, M.L. Liu, J. Power Sources 139 (2005) 314–320.
[8] S.L. Chou, J.Z. Wang, M. Choucair, H.K. Liu, J.A. Stride, S.X. Dou, Electrochem. Commun. 12 (2010) 303–306.
[9] Z.P. Guo, Z.W. Zhao, H.K. Liu, S.X. Dou, J. Power Sources 146 (2005) 190–194.
[10] W. Chen, Z.L. Fan, A. Dhanabalan, C.H. Chen, C.L. Wang, J. Electrochem. Soc. 158 (2011) A1055–A1059.
[11] W. Stöber, A. Fink, J. Colloid Interface Sci. 26 (1968) 62–69.
[12] C. Real, M.D. Alcalá, J.M. Criado, J. Am. Ceram. Soc. 79 (1996) 2012–2016.
[13] T. Zhang, J. Gao, H.P. Zhang, L.C. Yang, Y.P. Wu, H.Q. Wu, Electrochem. Commun. 9 (2007) 886–890.
[14] J.C. Guo, C.S. Wang, Chem. Commun. 46 (2010) 1428–1430.
[15] J.C. Guo, A. Sun, C.S. Wang, Electrochem. Commun. 12 (2010) 981–984.
[16] L.C. Yang, Q.S. Gao, Y.H. Zhang, Y. Tang, Y.P. Wu, Electrochem. Commun. 10 (2008) 118–122.
[17] Y.F. Shi, B.K. Guo, S.A. Corr, Q.H. Shi, Y.S. Hu, K.R. Heier, L.Q. Chen, R. Seshadri, G.D. Stucky, Nano Lett. 9 (2009) 4215–4220.
[18] J. Li, J.R. Dahn, J. Electrochem. Soc. 154 (2007) A156–A161.